REFERENCES

[1] L. O. Chua and L. Yang, "Cellular neural networks: Theory," *IEEE Trans. Circuits Syst.*, vol. 35, pp. 1257–1272, June 1988.

[2] ——, "Cellular neural networks: Applications," *IEEE Trans. Circuits Syst.*, vol. 35, pp. 1273–1290, June 1988.

[3] M. Joy, "On the global convergence of a class of functional differential equations with applications in neural network theory," *J. Math. Anal. Applicat.*, vol. 232, pp. 61–81, 1999.

[4] J. M. Cruz and L. O. Chua, "Design of high-speed, high density CNN's in CMOS technology," in *Cellular Neural Networks*, T. Roska and J. Vandewalle, Eds. London, U.K.: Wiley, 1993, pp. 117–134.

[5] X. Y. Wu, H. Chen, W. Tan, and W. K. Chen, "The improvement of the hardware design of artificial CNN and a fast algorithm of CNN component detector," *J. Franklin Institute*, vol. 330, pp. 1005–1015, 1993.

[6] P. P. Civalleri, L. M. Gilli, and L. Pabdolfi, "On stability of cellular neural networks with delay," *IEEE Trans. Circuits Syst. I*, vol. 40, pp. 157–164, Mar. 1993.

[7] T. Roska and L. O. Chua, "Cellular neural networks with nonlinear and delay-type template," *Int. J. Circuit Theory Appl.*, vol. 20, pp. 469–481, 1992.

[8] S. Arik and V. Tavsanoglu, "Equilibrium analysis of delayed CNNs," *IEEE Trans. Circuits Syst. I*, vol. 45, pp. 168–171, Feb. 1998.

[9] T. Roska, C. W. Wu, M. Balsi, and L. O. Chua, "Stability of cellular neural networks with dominant nonlinear and delay-type templates," *IEEE Trans. Circuits Syst. I*, vol. 40, pp. 270–272, Apr. 1993.

[10] T. L. Liao and F. C. Wang, "Global stability condition for cellular neural networks with time delay," in *Proc. 2000 Automatic Control Conf.*, 2000, pp. 493–497.

[11] Q. Zhang, R. Ma, and J. Xu, "Stability of cellular neural networks with delay," *Electron. Lett.*, vol. 37, no. 9, pp. 575–576, 2001.

[12] J. Cao, "Global stability analysis in delayed cellular neural networks," *Phy. Rev. E.*, vol. 59, pp. 5940–5944, 1999.

[13] M. S. Mahmoud and N. F. Al-Muthairi, "Design of robust controllers for time-delay systems," *IEEE Trans. Automat. Control*, vol. 39, pp. 995–999, May 1994.

[14] V. Kolmanovskii and A. Myshkis, *Introduction to the Theory and Applications of Functional Differential Equations*. Norwell, MA: Kluwer, 1999.

[15] S. Boyd, L. G. Ei, E. Feron, and V. Balakrishnan, *Linear Matrix Inequalities in System and Control Theory*. Philadelphia, PA: SIAM, 1994.

Study of Low-Frequency Bifurcation Phenomena of a Parallel-Connected Boost Converter System Via Simple Averaged Models

H. H. C. Iu and C. K. Tse

Abstract—This brief attempts to study the low-frequency bifurcation phenomena of a system of parallel-connected dc/dc boost converters. Analysis of the averaged state equations shows that the system loses stability via a Hopf bifurcation. The loci of eigenvalues and the local trajectories are studied. Computer simulations and experiments are performed to capture the effects of variation of some chosen parameters on the qualitative behavior of the system. In particular, it is shown that simple averaged models can be used to predict the occurrence of Hopf bifurcation in such systems.

Index Terms—Averaged models, Hopf bifurcation, parallel-connected dc/dc converters.

I. INTRODUCTION

Recently, paralleling converters has become a popular technique in power supply design for improving power processing capability, reliability, and flexibility. Being a nonlinear system, a parallel-connected system of converters can behave in many ways that are not predictable by conventional linear design and analysis methods. Bifurcations, for instance, are particularly relevant problems to engineers since they directly affect reliability and the usable ranges of operation. In this brief, we study the bifurcation phenomena of a parallel system of boost dc/dc converters using a simple averaged modeling approach [1]. Our objective is to show how "low-frequency" bifurcations can be systematically analyzed using simple averaged models. By "low-frequency" bifurcations, we mean those characterized by the birth of low-frequency orbits and hence capturable by averaged models.

Bifurcation behavior in dc/dc converter systems is usually studied via a discrete-time approach [2]–[5], which gives almost complete information about the system's dynamics. Bifurcation in parallel-connected converters can also be studied by using such an approach [6]. However, the mathematics involved is rather complicated. In this brief, we use a simple averaged model to study a system of parallel-connected boost converters.

II. MASTER–SLAVE CONTROLLED PARALLEL-CONNECTED DC/DC CONVERTERS

The system under study consists of two dc/dc converters which are connected in parallel feeding a common load. The current drawn by the load is shared properly between the two boost converters by the action of a master–slave control scheme [7]–[10]. Fig. 1 shows the block diagram of this master–slave configuration.

As shown in Fig. 1, two converters are controlled via a simple pulsewidth modulation (PWM) scheme, in which a control voltage
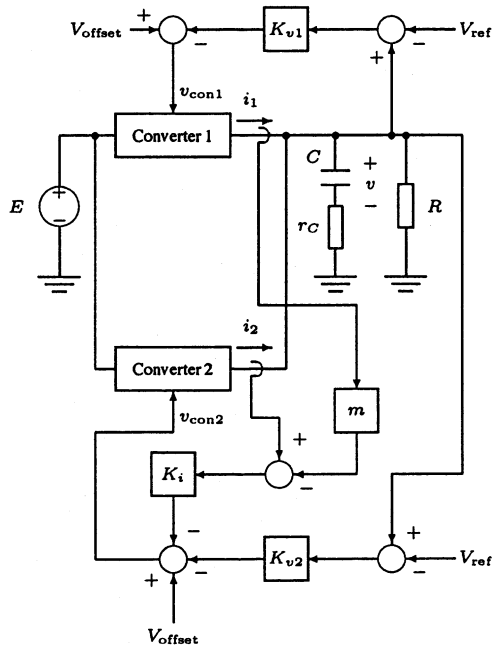
Fig. 1.　Block diagram of parallel-connected dc/dc converters under a master–slave control.
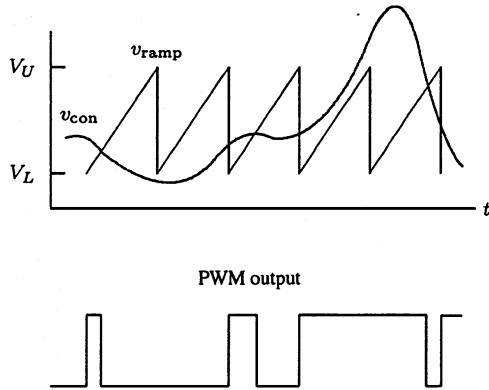

Fig. 2.　PWM showing relationship between the control voltage and the PWM output.

v_{con} is compared with a sawtooth signal to generate a pulsewidth-modulated signal that drives the switch, as shown in Fig. 2. The sawtooth signal of the PWM generator is given by

$$v_{\text{ramp}} = V_L + (V_U - V_L)\frac{t \bmod T}{T} \tag{1}$$

where V_L and V_U are the lower and upper voltage limits of the ramp, and T is the switching period. The PWM output is "high" when the control voltage is greater than v_{ramp} and is "low" otherwise. The control voltage for Converters 1 and 2 are given by

$$v_{\text{con}1} = V_{\text{offset}} - K_{v1}(v - V_{\text{ref}}) \tag{2}$$
$$v_{\text{con}2} = V_{\text{offset}} - K_{v2}(v - V_{\text{ref}}) - K_i(i_2 - mi_1) \tag{3}$$

where V_{offset} is a dc offset voltage that gives the steady-state duty cycle, V_{ref} is the reference voltage, K_{v1} is the voltage feedback gain for Converter 1, K_{v2} is the voltage feedback gain of Converter 2, K_i is the current feedback gain, and m is a current weighting factor. Under this scheme, the output current of Converter 2 will follow that of Converter 1 at a ratio of m to 1, where $m > 0$. When $m = 1$, we expect equal current sharing. In this brief, we assume $m = 1$. In much of the literature, Converter 1 is referred to as the "master" which operates independently and Converter 2 the "slave" which imitates the master's current value.
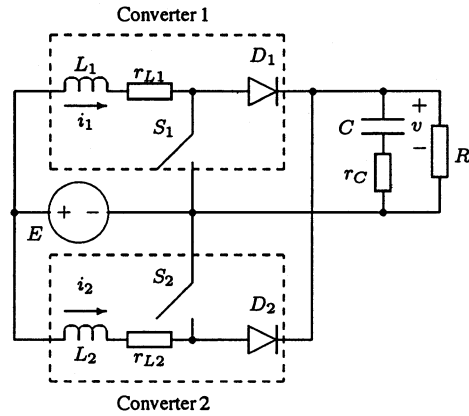

Fig. 3.　Two parallel-connected boost converters.

We now consider the special case where both converters are of the boost-type, as shown in Fig. 3. The presence of four switches (S_1, S_2, D_1 and D_2) allows a total of 16 possible switch states, and in each switch state, the circuit is a linear third-order circuit.

When the converters are operating in continuous conduction mode, diode D_i is always in complementary state to switch S_i, for $i = 1$, 2. That is, when S_i is on, D_i is off, and vice versa. Hence, only four switch states are possible during a switching cycle, namely (i) S_1 and S_2 are on; (ii) S_1 is on and S_2 is off; (iii) S_1 is off and S_2 is on; (iv) S_1 and S_2 are off. The state equations corresponding to these switch states are given by

$$\dot{x} = A_1 x + B_1 E, \quad \text{for } S_1 \text{ and } S_2 \text{ on}$$
$$\dot{x} = A_2 x + B_2 E, \quad \text{for } S_1 \text{ on and } S_2 \text{ off}$$
$$\dot{x} = A_3 x + B_3 E, \quad \text{for } S_1 \text{ off and } S_2 \text{ on}$$
$$\dot{x} = A_4 x + B_4 E, \quad \text{for } S_1 \text{ and } S_2 \text{ off} \tag{4}$$

where E is the input voltage, x is the state vector defined as

$$x = \begin{bmatrix} i_1 & i_2 & v \end{bmatrix}^T \tag{5}$$

and the A's and B's are given by

$$A_1 = \begin{bmatrix} -\frac{r_{L1}}{L_1} & 0 & 0 \\ 0 & -\frac{r_{L2}}{L_2} & 0 \\ 0 & 0 & -\frac{1}{C(R+r_C)} \end{bmatrix} \tag{6}$$

$$A_2 = \begin{bmatrix} -\frac{r_{L1}}{L_1} & 0 & 0 \\ 0 & -\frac{1}{L_2}\left(\frac{r_C R}{R+r_C} + r_{L2}\right) & -\frac{R}{L_2(R+r_C)} \\ 0 & \frac{R}{C(R+r_C)} & -\frac{1}{C(R+r_C)} \end{bmatrix} \tag{7}$$

$$A_3 = \begin{bmatrix} -\frac{1}{L_1}\left(\frac{r_C R}{R+r_C} + r_{L1}\right) & 0 & -\frac{R}{L_1(R+r_C)} \\ 0 & -\frac{r_{L2}}{L_2} & 0 \\ \frac{R}{C(R+r_C)} & 0 & -\frac{1}{C(R+r_C)} \end{bmatrix} \tag{8}$$

and by (9), shown at the bottom of the next page, and

$$B_1 = B_2 = B_3 = B_4 = \begin{bmatrix} \frac{1}{L_1} \\ \frac{1}{L_2} \\ 0 \end{bmatrix}. \tag{10}$$

It is worth noting that the sequence of switch states, in general, takes the order as written in (4), i.e., starting with "S_1 and S_2 on" and ending with "S_1 and S_2 off" in a switching cycle. However, either "S_1 on S_2 off" or "S_1 off S_2 on" (not both) goes in the middle, depending upon the duty cycles of S_1 and S_2. In the case where S_1 has a larger duty cycle, we should omit the third equation in (4) and likewise for the case where S_2 has a larger duty cycle. This should be taken care of in the simulation and analysis.
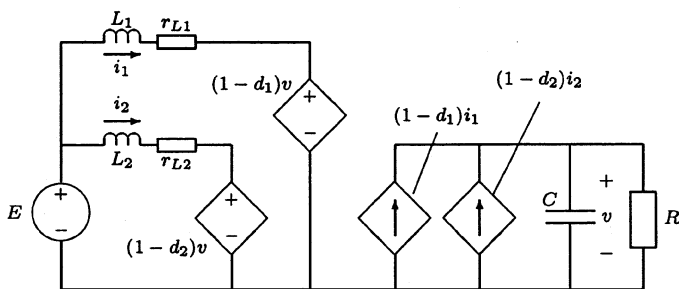
Fig. 4.   Averaged model of parallel-connected boost converters.

III. AVERAGED MODEL FOR TWO PARALLEL BOOST CONVERTERS

A. Derivation of Autonomous State Equations

The averaged model for the parallel-connected boost converters is shown in Fig. 4. The system can be represented by the averaged equations

$$
\begin{aligned}
\frac{di_1}{dt} &= \frac{-\left(1-d_1\right)v}{L_1} + \frac{E}{L_1} \\
\frac{di_2}{dt} &= \frac{-\left(1-d_2\right)v}{L_2} + \frac{E}{L_2} \\
\frac{dv}{dt} &= \frac{\left(1-d_1\right)i_1}{C} + \frac{\left(1-d_2\right)i_2}{C} - \frac{v}{RC}
\end{aligned}
\tag{11}
$$

where d_1 and d_2 are the duty cycles of Converters 1 and 2, respectively. We assume that r_{L1}, r_{L2} and r_C are zero in order to simplify the subsequent analysis. The duty cycles d_1 and d_2 can also be represented by

$$
\begin{aligned}
d_1 &= D - k_{v1}\left(v - V_{\mathrm{ref}}\right) \tag{12} \\
d_2 &= D - k_{v2}\left(v - V_{\mathrm{ref}}\right) - k_i\left(i_2 - i_1\right) \tag{13}
\end{aligned}
$$

where D is the steady-state duty cycle $k_{v1} = K_{v1}/(V_U - V_L)$, $k_{v2} = K_{v2}/(V_U - V_L)$, and $k_i = K_i/(V_U - V_L)$. It should be noted that $0 < d_1 < 1$ and $0 < d_2 < 1$ should be satisfied. Putting (12) and (13) into (11), we get the following autonomous equations that describe the dynamics of the system:

$$
\begin{aligned}
\frac{di_1}{dt} &= \frac{-\left(1-D+k_{v1}\left(v-V_{\mathrm{ref}}\right)\right)v}{L_1} + \frac{E}{L_1} \\
\frac{di_2}{dt} &= \frac{-\left(1-D+k_{v2}\left(v-V_{\mathrm{ref}}\right)+k_i\left(i_2-i_1\right)\right)v}{L_2} + \frac{E}{L_2} \\
\frac{dv}{dt} &= \frac{\left(1-D+k_{v1}\left(v-V_{\mathrm{ref}}\right)\right)i_1}{C} \\
&\quad + \frac{\left(1-D+k_{v2}\left(v-V_{\mathrm{ref}}\right)+k_i\left(i_2-i_1\right)\right)i_2}{C} - \frac{v}{RC}.
\end{aligned}
\tag{14}
$$

The autonomous equations are valid only when $0 < d_1 < 1$ and $0 < d_2 < 1$. Such conditions are satisfied when the system is operating in the stable equilibrium state or in the neighborhood of the equilibrium state.

B. Dimensionless Equations

The afore-derived state equations can be put in a dimensionless form. We define the dimensionless state variables as follows:

$$
x_1 = \frac{i_1 R}{V_{\mathrm{ref}}}, \; x_2 = \frac{i_2 R}{V_{\mathrm{ref}}}, \; x_3 = \frac{v}{V_{\mathrm{ref}}}. \tag{15}
$$

We also define the dimensionless time and parameters as follows:

$$
\begin{aligned}
\tau &= \frac{t}{T}, \; \xi_1 = \frac{L_1}{RT}, \; \xi_2 = \frac{L_2}{RT}, \; \zeta = \frac{CR}{T} \\
\kappa_{v1} &= k_{v1} V_{\mathrm{ref}}, \; \kappa_{v2} = k_{v2} V_{\mathrm{ref}}, \; \kappa_i = \frac{k_i V_{\mathrm{ref}}}{R} e = \frac{E}{V_{\mathrm{ref}}}. \tag{16}
\end{aligned}
$$

Direct substitution of these new dimensionless variables, time and parameters in the autonomous (14) yields the dimensionless autonomous equations (17), shown at the bottom of the page. Now, (12) and (13) can be written as

$$
\begin{aligned}
d_1 &= D - \kappa_{v1}\left(x_3 - 1\right) \tag{18} \\
d_2 &= D - \kappa_{v2}\left(x_3 - 1\right) - \kappa_i\left(x_2 - x_1\right). \tag{19}
\end{aligned}
$$

To complete the model, saturation must be included. When $d_1 < 0$ or/and $d_2 < 0$, we put $d_1 = 0$ or/and $d_2 = 0$ in (11) and perform dimensionless substitution. Similarly, when $d_1 > d_{\max}$ or/and $d_2 > d_{\max}$, we put $d_1 = d_{\max}$ or/and $d_2 = d_{\max}$ in (11) and perform dimensionless substitution.

C. Equilibrium Point Calculation

The equilibrium point can be calculated by setting all time-derivatives in (17) to zero and solving for x_1, x_2 and x_3. This gives

$$
X = \begin{bmatrix} X_1 \\ X_2 \\ X_3 \end{bmatrix} = \begin{bmatrix} \frac{1}{2e} \\ \frac{1}{2e} \\ 1 \end{bmatrix} \tag{20}
$$

where $e = 1 - D$.

IV. STABILITY OF EQUILIBRIUM POINT AND HOPF BIFURCATION

The Jacobian $J(X)$ for the dimensionless system evaluated at the equilibrium point is given by

$$
J(X) = \begin{bmatrix}
0 & 0 & \frac{-(\kappa_{v1}+1-D)}{\xi_1} \\
\frac{\kappa_i}{\xi_2} & \frac{-\kappa_i}{\xi_2} & \frac{-(\kappa_{v2}+1-D)}{\xi_2} \\
\frac{2e(1-D)-\kappa_i}{2e\zeta} & \frac{2e(1-D)+\kappa_i}{2e\zeta} & \frac{\kappa_{v1}+\kappa_{v2}-2e}{2e\zeta}
\end{bmatrix}. \tag{21}
$$

We attempt to study the stability of the equilibrium point and the trajectory in the neighborhood of the equilibrium point by deriving the

$$
A_4 = \begin{bmatrix}
-\frac{1}{L_1}\left(\frac{r_C R}{R+r_C} + r_{L1}\right) & 0 & -\frac{R}{L_1(R+r_C)} \\
0 & -\frac{1}{L_2}\left(\frac{r_C R}{R+r_C} + r_{L2}\right) & -\frac{R}{L_2(R+r_C)} \\
\frac{R}{C(R+r_C)} & \frac{R}{C(R+r_C)} & -\frac{1}{C(R+r_C)}
\end{bmatrix} \tag{9}
$$

$$
\begin{aligned}
\frac{dx_1}{d\tau} &= \frac{e - \left(1 - D + \kappa_{v1}\left(x_3 - 1\right)\right)x_3}{\xi_1} \\
\frac{dx_2}{d\tau} &= \frac{e - \left(1 - D + \kappa_{v2}\left(x_3 - 1\right) + \kappa_i\left(x_2 - x_1\right)\right)x_3}{\xi_2} \\
\frac{dx_3}{d\tau} &= \frac{\left(1 - D + \kappa_{v1}\left(x_3 - 1\right)\right)x_1 + \left(1 - D + \kappa_{v2}\left(x_3 - 1\right) + \kappa_i\left(x_2 - x_1\right)\right)x_2 - x_3}{\zeta}
\end{aligned}
\tag{17}
$$

TABLE I
EIGENVALUES FOR INCREASING VALUE OF κ_{v2} ($\kappa_{v1} = 0.48$ AND $\kappa_i = 0.40$)

κ_{v2}	Eigenvalues	Remarks
0.340	$-0.0330 \pm j0.1810$, -0.0460	Stable equilibrium point
0.380	$-0.0260 \pm j0.1870$, -0.0440	Stable equilibrium point
0.420	$-0.0190 \pm j0.1920$, -0.0420	Stable equilibrium point
0.460	$-0.0120 \pm j0.1960$, -0.0410	Stable equilibrium point
0.500	$-0.0044 \pm j0.2000$, -0.0390	Stable equilibrium point
0.540	$0.0030 \pm j0.2030$, -0.0380	Unstable equilibrium point

eigenvalues of the system at the equilibrium point. The usual procedure is to solve the following equation for λ:

$$\det[\lambda \mathbf{1} - J(X)] = 0. \tag{22}$$

Upon expanding, we get

$$\lambda^3 + \left(\frac{\kappa_i}{\xi_2} - \frac{\kappa_{v1} + \kappa_{v2} - 2e}{2e\zeta} \right) \lambda^2$$
$$+ \left[\left(\frac{\kappa_{v2} + 1 - D}{\xi_2} \right) \left(\frac{2e(1-D) + \kappa_i}{2e\zeta} \right) \right.$$
$$+ \left(\frac{2e(1-D) - \kappa_i}{2e\zeta} \right) \left(\frac{\kappa_{v1} + 1 - D}{\xi_1} \right)$$
$$\left. - \left(\frac{\kappa_i}{\xi_2} \right) \left(\frac{\kappa_{v1} + \kappa_{v2} - 2e}{2e\zeta} \right) \right] \lambda$$
$$+ \left[\left(\frac{\kappa_i}{\xi_2} \right) \left(\frac{\kappa_{v1} + 1 - D}{\xi_1} \right) \left(\frac{2(1-D)}{\zeta} \right) \right] = 0. \tag{23}$$

Using the above equation, the following conditions are easily verified:

$$\lim_{\lambda \to -\infty} \det[\lambda \mathbf{1} - J(X)] \to -\infty \tag{24}$$

$$\det[-J(X)] > 0. \tag{25}$$

Hence, there exists at least one $\lambda \in (-\infty, 0)$ such that $\det[\lambda \mathbf{1} - J(X)] = 0$, i.e., the system has at least one negative real eigenvalue. Also, numerical calculations of eigenvalues for the practical range of parameters ($\xi_1 = \xi_2 = 10$, $\zeta = 2.5$, $e = 0.5$ and $D = 0.5$) reveal that the other two eigenvalues are a complex conjugate pair which have either a positive or negative real part depending upon values of κ_{v1} and κ_{v2}. In particular, the following observations are made.

1) For small values of κ_{v1} and κ_{v2}, the pair of eigenvalues has a negative real part.
2) As κ_{v1} or/and κ_{v2} increases, the real part of the complex eigenvalues get less negative and at a critical value of κ_{v1} or/and κ_{v2}, the real part changes from negative to positive. Table I shows a typical scenario of the variation of the eigenvalues. The loci is plotted in Fig. 5 for ease of reference.
3) The critical value of κ_{v1} or/and κ_{v2} depends on the values of ξ_1, ξ_2, ζ, e, D and κ_i. As we increase κ_{v1} or/and κ_{v2}, the sign of the real part of the complex eigenvalues changes, the system loses stability via a *Hopf bifurcation* [11].

V. LOCAL TRAJECTORIES FROM THE AVERAGED EQUATIONS

In this section, we re-examine the stability in terms of the local trajectories near the equilibrium point. Since the use of an averaged model for predicting nonlinear phenomena will become inadequate when stability is lost, our aim in this section is to observe, by plotting the local trajectories, the behavior of the system as it goes from a stable region to an unstable region. For further investigation beyond the bifurcation point predicted by the averaged model, we need to resort to the exact piecewise switched model, as will be reported in Section VI.
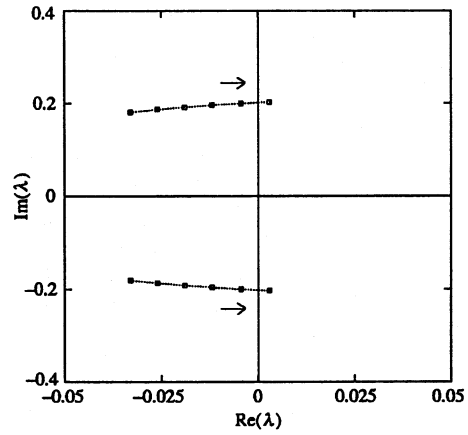

Fig. 5. Loci of the complex eigenvalue pair moving from left to right as K_{v2} increases.

The trajectory of the system near the equilibrium point can be easily derived from the corresponding eigenvalues and eigenvectors. Suppose the eigenvalues and their corresponding eigenvectors are

$$\lambda_r, \ \sigma \pm j\omega \text{ and } \bar{v}_r, \ \bar{v}_1 \pm j\bar{v}_2. \tag{26}$$

The solution in general is given by

$$\mathbf{x}(t) = c_r e^{\lambda_r t} \bar{v}_r + 2c_c e^{\sigma t} \left[\cos(\omega t + \phi_c) \bar{v}_1 - \sin(\omega t + \phi_c) \bar{v}_2 \right] \tag{27}$$

where c_r, c_c, and ϕ_c are determined by initial conditions. The geometry of the trajectory is best described in terms of the eigenline L_r, which is parallel to $\bar{v}_r$, and the eigenplane E_c, which is spanned by $\bar{v}_1$ and $\bar{v}_2$, the intersection of L_r and E_c being the equilibrium point. Essentially, since the real eigenvalue is negative, the system moves initially in the direction of L_r going toward E_c. At the same time it moves in a helical motion converging toward or diverging away from L_r, depending upon the sign of the real part of the complex eigenvalues. As it lands on E_c, it keeps spiraling along E_c toward or away from the equilibrium point. The following examples illustrate two typical local trajectories, corresponding to a stable and an unstable equilibrium point.

We first examine the stable system with $\kappa_{v1} = 0.48$, $\kappa_{v2} = 0.45$ and $\kappa_i = 0.40$. The Jacobian evaluated at the equilibrium point is

$$J(X) = \begin{bmatrix} 0 & 0 & -0.098 \\ 0.04 & -0.04 & -0.095 \\ 0.04 & 0.36 & -0.028 \end{bmatrix}. \tag{28}$$

The eigenvalues λ and their corresponding eigenvectors $\bar{v}$, are found as

$$\lambda = -0.041, -0.013 \pm j0.195 \tag{29}$$

$$\bar{v} = \begin{bmatrix} 0.916 \\ -0.116 \\ 0.384 \end{bmatrix}, \begin{bmatrix} 0.028 \pm j0.410 \\ 0.030 \pm j0.398 \\ 0.820 \end{bmatrix}. \tag{30}$$

A three-dimensional (3-D) view of the trajectory is shown in Fig. 6.

We next examine the unstable system with $\kappa_{v1} = 0.48$, $\kappa_{v2} = 0.55$, and $\kappa_i = 0.40$. The system loses stability. The Jacobian evaluated at the equilibrium point is

$$J(X) = \begin{bmatrix} 0 & 0 & -0.098 \\ 0.04 & -0.04 & -0.105 \\ 0.04 & 0.36 & 0.012 \end{bmatrix}. \tag{31}$$

The eigenvalues λ and their corresponding eigenvectors $\bar{v}$ are found as

$$\lambda = -0.038, 0.00484 \pm j0.204 \tag{32}$$

$$\bar{v} = \begin{bmatrix} 0.923 \\ -0.151 \\ 0.355 \end{bmatrix}, \begin{bmatrix} 0.00933 \pm j0.393 \\ 0.015 \pm j0.420 \\ 0.818 \end{bmatrix}. \tag{33}$$
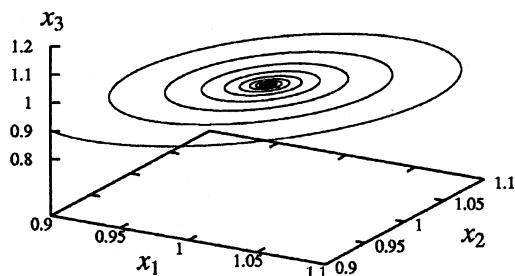
Fig. 6. View of the stable (spiralling inward) local trajectory from the averaged model ($\kappa_{v1} = 0.48$, $\kappa_{v2} = 0.45$, and $\kappa_i = 0.40$).
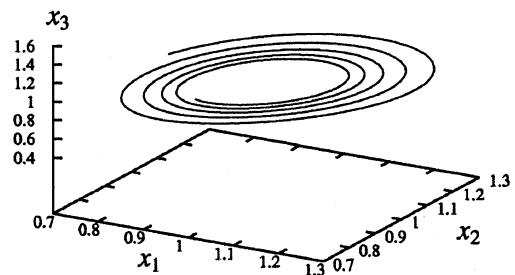

Fig. 7. View of the unstable (spiralling outward) local trajectory from the averaged model ($\kappa_{v1} = 0.48$, $\kappa_{v2} = 0.55$ and $\kappa_i = 0.40$).
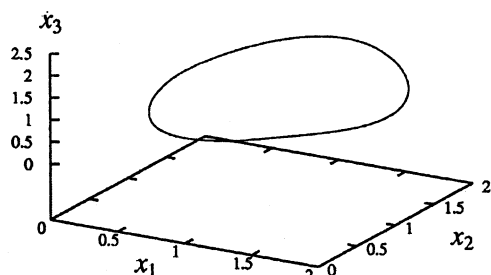

Fig. 8. Limit cycle from the averaged model ($\kappa_{v1} = 0.48$, $\kappa_{v2} = 0.55$, and $\kappa_i = 0.40$).

A 3-D view of the trajectory is shown in Fig. 7. In Fig. 8, we also observe that the trajectory settles down into a limit cycle after the transient period.

From the above examples, we clearly observe that the system loses stability via a Hopf bifurcation. Before the bifurcation, the local trajectory spirals into the equilibrium point. After the bifurcation, the local trajectory spirals away from the equilibrium point and settles down into a limit cycle.

VI. COMPUTER SIMULATION STUDY

Since the foregoing analysis is based on a set of nonlinear state equations which is derived from an averaged continuous model, it falls short of predicting the details after the bifurcation. In this section, we examine the system using computer simulation which employs an exact piecewise switched model. Essentially, using the state equations in Section II, cycle-by-cycle simulations are performed to emulate the exact original system. In our simulations, we include suitable algorithms to take into account possible of the circuit into discontinuous conduction mode (DCM). Thus the simulation results represent viable verification of the behavior of the real circuit.

Since we are primarily concerned with system stability in conjunction with the feedback design, we will focus our attention on the effects of varying the various gains on the bifurcation behavior of the system.

TABLE II
COMPONENT VALUES AND STEADY-STATE VOLTAGES USED IN SIMULATION.
(ESR STANDS FOR EQUIVALENT SERIES RESISTANCE)

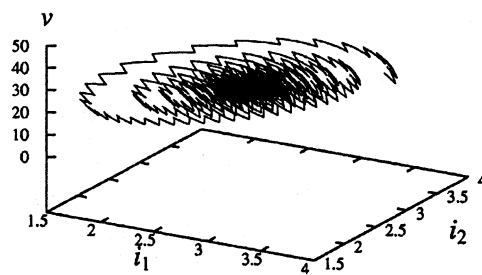| Circuit Components	Values
Switching Period T	$40\mu s$
Input Voltage E	12V
Output Voltage v	24V
Reference Voltage V_{ref}	24V
Inductance L_1, ESR r_{L1}	$0.004H, 0.05\Omega$
Inductance L_2, ESR r_{L2}	$0.004H, 0.2\Omega$
Capacitance C, ESR r_C	$10\mu F, 0.01\Omega$
Load Resistance R	10Ω

Fig. 9. View of the stable (spiralling inward) local trajectory from the exact piecewise switched model.
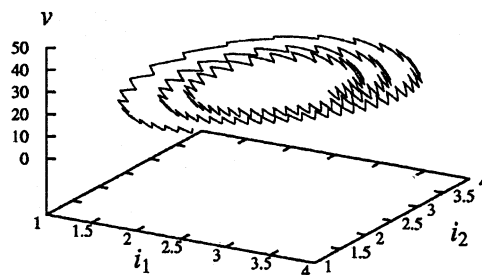

Fig. 10. View of the unstable (spiralling outward) local trajectory from the exact piecewise switched model.
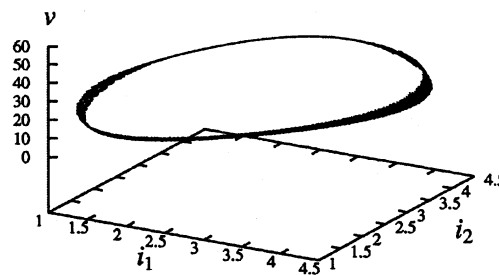

Fig. 11. Quasi-periodic orbit from the exact piecewise switched model.

In particular, the gains K_{v1}, K_{v2}, and K_i present themselves as design parameters that can be changed at will. We will henceforth focus on variation of these parameters.

Our simulation is based on the exact state equations derived in Section II. Essentially, for each set of parameter values, time-domain cycle-by-cycle waveforms are generated by solving the appropriate linear equation in any sub-interval of time, according to the states of the switches which are determined from values of the control voltages $v_{\text{con}1}$ and $v_{\text{con}2}$. Sampled data are then collected at $t = nT$ in the steady state. With sufficient number of sets of steady-state data, we can construct the bifurcation diagrams as required. Our computer program automatically organizes bifurcation diagrams from time-domain waveforms. The circuit parameters used in our simulations are shown in Table II.
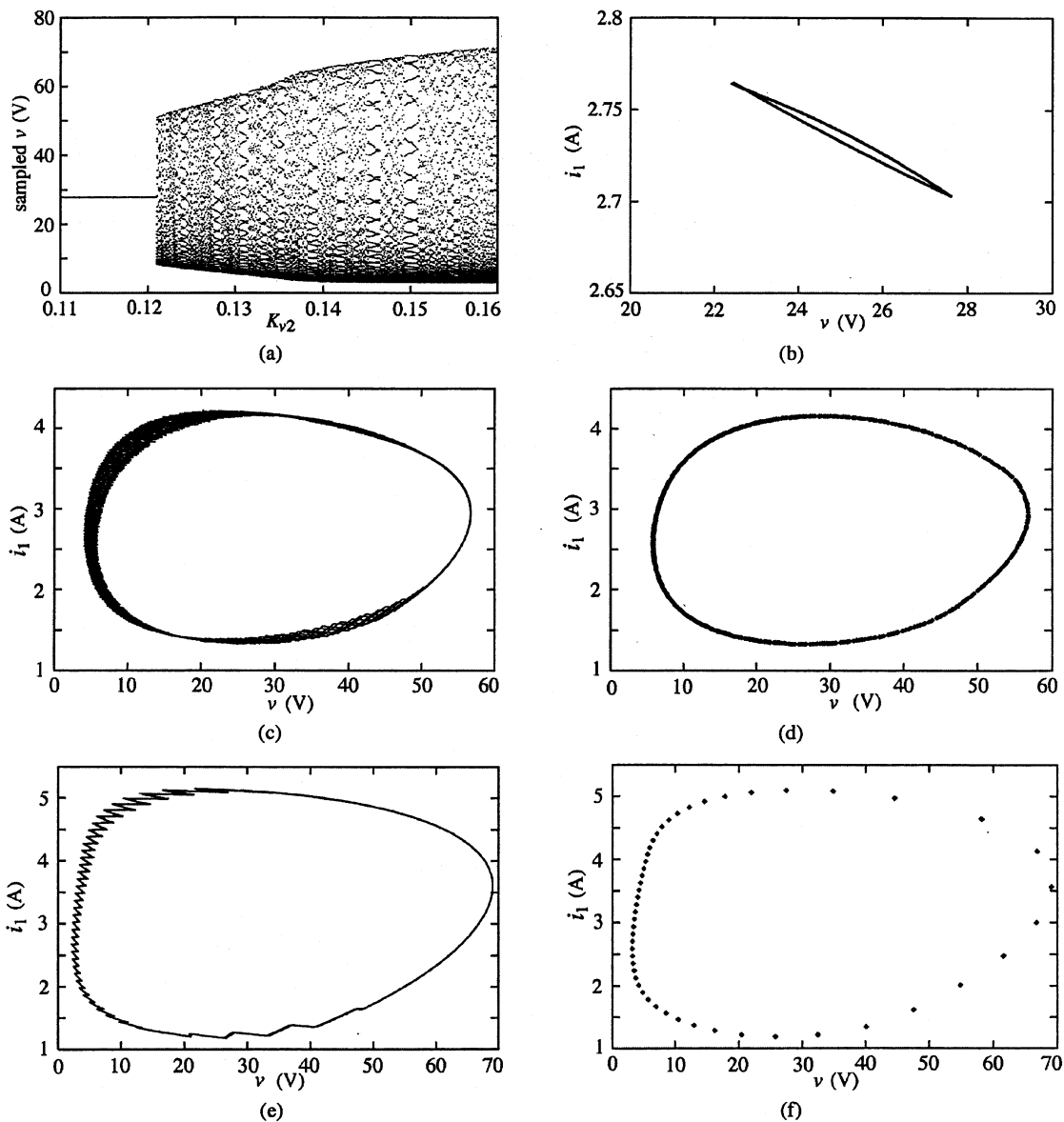
Fig. 12. (a) Bifurcation diagram with K_{v2} as bifurcation parameter ($K_{v1} = 0.11$ and $K_i = 1$). (b) Stable period-1 orbit ($K_{v1} = 0.11$, $K_{v2} = 0.11$ and $K_i = 1$). (c) Quasi-periodic orbit ($K_{v1} = 0.11$, $K_{v2} = 0.13$ and $K_i = 1$). (d) Stroboscopic map of (c). (e) Limit cycle ($K_{v1} = 0.11$, $K_{v2} = 0.15$ and $K_i = 1$). (f) Stroboscopic map of (e).

Since we are simulating the actual circuits, the original circuit parameters will be used instead of the dimensionless ones. In particular, we will focus on the qualitative change of dynamics as K_{v1} or/and K_{v2} is varied. To observe the trend, we keep K_{v1} constant and vary K_{v2} (similar trend is observed when we keep K_{v2} constant and vary K_{v1}). A summary of the observed behavior is as follows.

1) When K_{v2} is small, the trajectory spirals into a fixed period-1 orbit, corresponding to a fixed point in the averaged system. Fig. 9 shows the simulated trajectory.
2) When K_{v2} is increased beyond a critical value, the period-1 orbit becomes unstable and the trajectory spirals outward as shown in Fig. 10, and settles into a quasi-periodic period, as shown in Fig. 11.

The above observations confirm the prediction we made in Section V based on the averaged equations.

In order to give a better view of the dynamics of the system after the Hopf bifurcation, a large number of trajectories and bifurcation diagrams have been obtained. In the following, only representative bifurcation diagrams and sequence of trajectories are shown, which serve to exemplify the main findings concerning the bifurcation behavior of a system of parallel boost converters under a master–slave current sharing scheme.

We first keep K_{v1} and K_i constant and vary K_{v2}. A bifurcation diagram is shown in Fig. 12(a). The sequence of simulated trajectories, as shown in Fig. 12(b), (c), and (e), reveals a typical Hopf bifurcation in which a stable equilibrium state breaks down to quasi-periodic orbits and limit cycles. The corresponding stroboscopic maps showing a quasi-periodic orbit and a limit cycle are shown in Fig. 12(d) and (f). Next, we keep K_{v2} and K_i constant and vary K_{v1}. Similar bifurcation diagram and trajectories are obtained. For brevity, they are not repeated here.

Remarks: In studying the bifurcation behavior in respect of current gain variation, we keep K_{v1} and K_{v2} constant and vary K_i. It is found that the system remains in stable period-1 operation irrespective of the
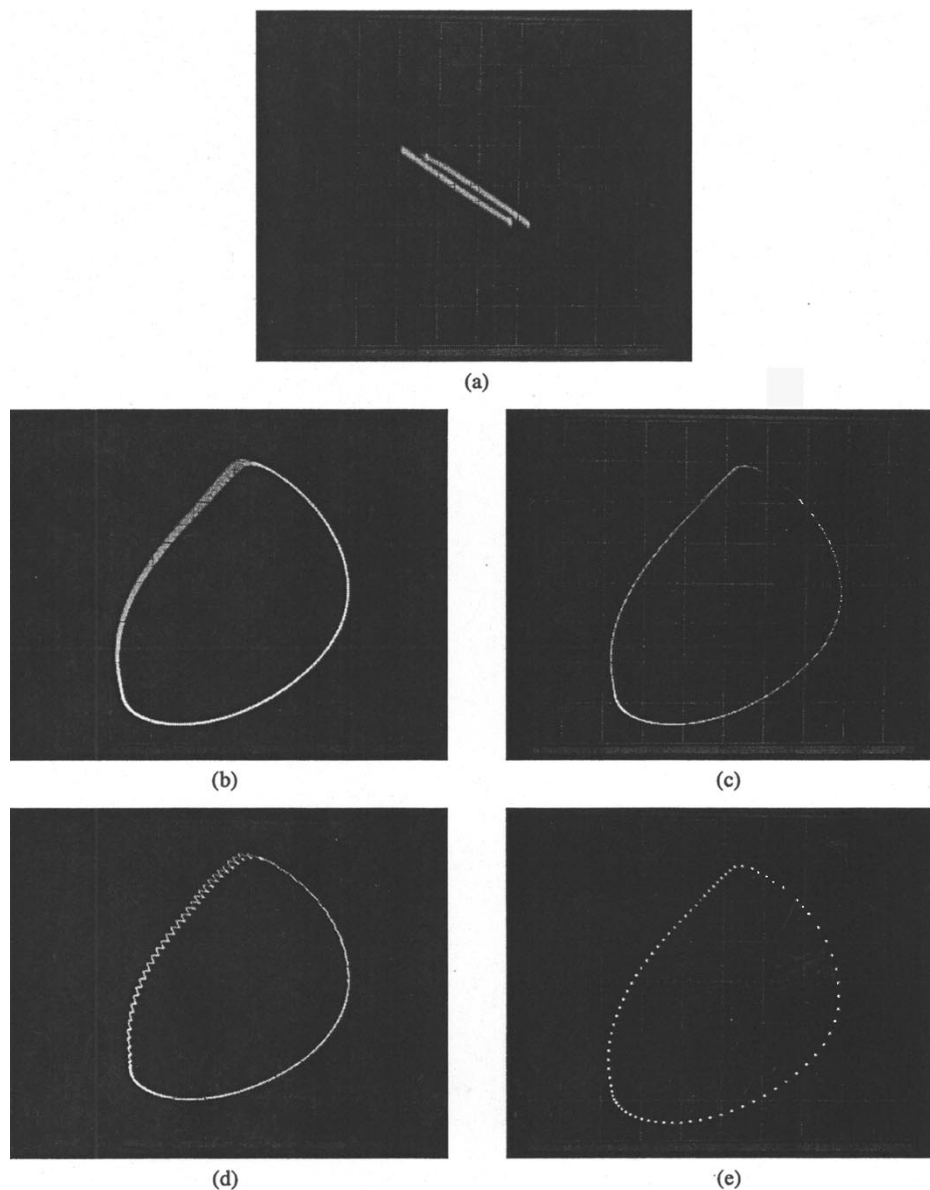
Fig. 13. Sequence of changes observed experimentally when K_{v2} is increased. (a) Stable period-1 orbit. (b) Quasi-periodic orbit. (c) Stroboscopic map of (b). (d) Limit cycle. (e) Stroboscopic map of (d). Horizontal scale: 5 V/div, vertical scale: 0.04 A/div for (a); Horizontal scale: 10 V/div, vertical scale: 0.4 A/div for (b)–(e)..

choice of K_i. Basically, K_i only determines how close the slave follows the master. The larger K_i is, the closer the slave's output current is to the master's.

VII. EXPERIMENTAL VERIFICATION

Using the parameter values listed in Table II, we have built a circuit to verify our simulation results. As we increase K_{v2}, we get results which are in good agreement with our simulations. In our experiments, Hopf bifurcation takes place at approximately the same location (in terms of the value of the dc gain) as it does in our simulations. Trajectories of stable period-1 orbit, quasi-periodic orbit and limit cycle are captured, along with stroboscopic maps showing quasi-periodic orbits and limit cycles. In all the oscilloscope pictures, y-axis corresponds to i_1 and x-axis corresponds to v. Fig. 13(a)–(e) show the sequence of changes when we increase K_{v2}. Fig. 13(a) shows a stable period-1 orbit, Fig. 13(b) shows a quasi-periodic orbit, and Fig. 13(c) gives its

stroboscopic map. Fig. 13(d) shows a limit cycle and Fig. 13(e) gives its stroboscopic map.

VIII. CONCLUSION

Despite the popularity of parallel converter systems in power electronics applications, their bifurcation phenomena are rarely studied [5]. This brief attempts to use an averaged model to explain some low-frequency nonlinear phenomena in a parallel system of two boost converters which share current under a master–slave control scheme. The study of stability is a complex issue in this type of system [8]–[10]. This brief focuses on the effects of variation of some voltage feedback gains. It has been found that Hopf bifurcation is possible when the voltage feedback gains are varied. In engineering design, stable period-1 operation is the only acceptable operation. Thus in practice, instability often refers to failure of the circuit in maintaining its operation in the expected stable period-1 regime. In this brief, we have identified the parameters that cause "instability" and analyzed the detailed bifurcation

behavior via simple averaged models. The results presented are useful for practical design of parallel boost converters to ensure operation in the expected stable region.

REFERENCES

[1] C. K. Tse, Y. M. Lai, and H. H. C. Iu, "Hopf bifurcation and chaos in a free-running current-controlled Ćuk switching regulator," *IEEE Trans. Circuits Syst. I*, vol. 47, pp. 448–457, Apr. 2000.
[2] D. C. Hamill, J. H. B. Deane, and D. J. Jefferies, "Modeling of chaotic dc/dc converters by iterative nonlinear mappings," *IEEE Trans. Power Electron.*, vol. 7, pp. 25–36, Jan. 1992.
[3] C. K. Tse, "Flip bifurcation and chaos in three-state boost switching regulators," *IEEE Trans. Circuits Syst. I*, vol. 41, pp. 16–23, Jan. 1994.
[4] M. di Bernardo and F. Vasca, "Discrete-time maps for the analysis of bifurcations and chaos in dc/dc converters," *IEEE Trans. Circuits Syst. I*, vol. 47, pp. 130–143, Feb. 2000.
[5] H. H. C. Iu and C. K. Tse, "Bifurcation behavior in parallel-connected buck converters," *IEEE Trans. Circuits Syst. I*, vol. 48, pp. 233–240, Feb. 2001.
[6] ——, "Bifurcation in parallel-connected boost dc/dc converters," in *Proc. IEEE Int. Symp. Circuits and Systems*, 2000, pp. II473–II476.
[7] K. Siri, C. Q. Lee, and T. F. Wu, "Current distribution control for parallel connected converters: Part I," *IEEE Trans. Aerospace Electron. Syst.*, vol. 28, pp. 829–840, July 1992.
[8] V. J. Thottuvelil and G. C. Verghese, "Analysis and control of paralleled dc/dc converters with current sharing," *IEEE Trans. Power Electron.*, vol. 13, pp. 635–644, July 1998.
[9] Y. Panov, J. Rajagopalan, and F. C. Lee, "Analysis and design of N paralleled DC-DC converters with master–slave current-sharing control," in *Rec. IEEE Appl. Power Electronics Conf.*, 1997, pp. 436–442.
[10] S. K. Mazumder, A. H. Nayfeh, and D. Boroyevich, "A nonlinear approach to the analysis of stability and dynamics of standalone and parallel DC-DC converters," in *Rec. IEEE Appl. Power Electronics Conf.*, 2001, pp. 784–790.
[11] K. T. Alligood, T. D. Sauer, and J. A. Yorke, *Chaos: An Introduction to Dynamical Systems*. New York: Springer-Verlag, 1996.

Chaotic Dynamics of an Integrate-and-Fire Circuit With Periodic Pulse-Train Input

Wei Lin and Jiong Ruan

Abstract—In this brief, we first introduce the working principle of a pacemaker neuron type integrate-and-fire circuit having two states with a periodic pulse-train input, which is first proposed by Nakano, Mitsubori, and Saito. The dynamics of this circuit could be described by a standard impulsive differential equation and applied to simulate the evolution of the pulse-coupled neural networks. By applying the Marotto theorem, we theoretically prove that the circuit becomes chaotic as the parameters enter some regions. we find that the circuit does not exhibit chaotic dynamics with some little period of the pulse-train input but it appears chaotic phenomenon with the increase of the period. The relations between this circuit and that of symbolic dynamics are further investigated. The following numerical simulations and corresponding calculation, as illustrative examples, reinforce our theoretical proof and theory.

Index Terms—Chaos, integrate and fire, snap-back repeller, symbolic dynamics.

I. INTRODUCTION

It is a well-established fact that the basic dynamics of a single neuron model is as follows "If the state reaches a threshold, it fires and is reset to a base level, instantaneously." This is so-called integrate and fire. Researchers, such as Keener [1], Glass [2], and their coworkers, have given a vast amount of meritorious results concerning the stable dynamics of integrate-and-fire neuron with oscillatory input. Given the integrate-and-fire models, we can easily construct pulse-coupled neural networks (PCNNs). It could be found that the PCNNs as well as the simple integrate-and-fire models exhibit a variety of dynamical phenomena such as mutual synchronization, asynchronization, and even chaos. Because of the great significance of PCNNs' application to nonlinear science, the neural information processing in brain, and even the information communication, many researchers, such as Hopfield [3], Mirollo [4], and their colleagues, in particular, devote their research to have a clear analysis of PCNNs' synchronization. Moreover, the dynamics of integrate-and-fire circuit could be directly implemented to simulate the dynamics of corresponding PCNNs. Nakano, Mitsubori, and Saito presented such an integrate-and-fire circuit with or without periodic pulse-train input. They investigated its basic dynamics, and deduced some results about synchronization and bifurcation to chaos of the pulse-coupling circuit and numerically calculated the Lyapunov Exponent [5]–[7]. Nakano and Saito [8] also analytically derived several conditions for chaos generation by proving the existence of the positive Lyapunove exponent (PLE). Moreover, Miyachi *et al.* in [9] by numerical PLE further investigated the chaotic dynamics in the circuit with periodic input.

Besides the above background of PCNNs, our work is also inspired by the research in [10]–[13] about chaotic dynamics in the discrete neural network systems and anti-control in discrete systems. In their